

Revealing Unconventional Properties of a Spin-Orbit Coupled Bose-Einstein Condensate from Collective Dipole Oscillation

Shuai Chen¹, Jin-Yi Zhang¹, Si-Cong Ji¹, Zhu Chen², Long Zhang¹, Zhi-Dong Du¹, You-Jin Deng¹, Hui Zhai², Jian-Wei Pan¹

¹*Hefei National Laboratory for Physical sciences at Microscale and Department of Modern Physics, University of Science and Technology of China, Hefei, Anhui 230027, PR China and*

²*Institute for Advanced Study, Tsinghua University, Beijing, 100084, China*

(Dated: October 31, 2016)

Abstract

Interaction between matter field and gauge field plays a fundamental role in many areas of physics. Recently, a non-abelian gauge field has been successfully synthesized in laboratory for ultracold neutral bosonic atoms, yielding the coupling between the pseudo-spin of an atom and its orbital motion. This new superfluid has many unconventional properties remaining to be explored. Here we study the collective oscillation of a spin-orbit coupled Bose-Einstein condensate in a harmonic trap. We find that the frequency of dipole oscillation deviates from the harmonic trap frequency and depends on the oscillation amplitude. Such an unharmonic behavior reveals the non-abelian character of the gauge field. We also observe that a magnetization oscillation is induced by the dipole motion, as a manifestation of the absence of the Galilean invariance of this system. We develop a variational wave-function method that well describes the dipole oscillation, except in the regime with two degenerate single-particle energy minima separated by a low barrier. In this regime, since the harmonic trapping potential plays an analogous role as kinetic energy in a real-space double-well potential, macroscopic quantum tunneling in momentum space is observed in the dipole oscillation.

PACS numbers:

Discovering new quantum states of matter is an important mission of condensed matter physics, and now is also an important goal for cold atom research. In the past decades, many interesting macroscopic quantum phases have been discovered in solid state materials when electrons are placed in a strong magnetic field or possess strong spin-orbit (SO) coupling, such as the fractional quantum Hall effect [1] and the topological insulator [2]. However, in cold atom systems, neutral atoms possess neither gauge coupling to electromagnetic fields nor SO coupling. Until recently, by means of Raman coupling technique, several experiments have successfully synthesized abelian and non-abelian gauge potentials in cold atom systems [3–8]. Synthetic gauge potentials, like optical lattices, are becoming a powerful tool for simulating real materials with cold atoms. Moreover, a non-abelian gauge field introduces the coupling between the orbital motion of the atoms and their spins, and leads to a new quantum system of SO coupled bosons, which does not have an analogy in any condensed matter systems studied before. Theoretically, SO coupled bosons are predicted to exhibit an unconventional striped superfluid phase [9, 10] with exotic properties [11], while most novel properties have not been experimentally studied yet.

Dynamic processes have been playing a very important role in studying physical properties of trapped atomic Bose-Einstein condensates (BEC) and degenerate Fermi gases. For examples, anisotropic expansion is taken as a direct evidence for the onset of BEC [12], the surface-mode frequency can be used to probe the hydrodynamic behavior [13], the precision measurement of the frequency of the compression mode has revealed beyond mean-field effects in the molecular condensate [14], and the heavily damped dipole mode of one-dimensional bosons in optical lattices reflects strong quantum fluctuations in lower dimension [15]. In this work we utilize the dipole oscillation to reveal several fundamental properties of a SO coupled BEC that are absent in conventional Bose condensates. Dipole motion is a center-of-mass oscillation of all atoms, of which the frequency is the harmonic trap frequency and is independent of interaction for a conventional condensate. This is known as Kohn theorem [16, 17]. However, in a SO coupled condensate we find that such an oscillation is no longer harmonic as a consequence of the non-abelian nature of the underlying gauge potential. We also find an oscillation of magnetization synchronized to the dipole oscillation, due to the absence of Galilean invariance of this system. When the system has two degenerate single-particle ground states, macroscopic quantum tunneling is also observed during dipole oscillation.

Before introducing the experimental details, we shall first explain why dipole oscillation is interesting and why it is connected to the fundamental properties of a SO coupled condensate. The quantum many-body Hamiltonian of our system can be written as

$$\hat{H} = \sum_{i=1}^N \sum_{\alpha=x,y,z} \left(\frac{1}{2m} (\hat{p}_{\alpha,i} - A_{\alpha})^2 + \Phi + \frac{1}{2} m \omega_{\alpha}^2 r_{\alpha,i}^2 \right) + \sum_{i<j} U(\mathbf{r}_i - \mathbf{r}_j), \quad (1)$$

where ω_{α} is the frequency of the harmonic trap and $U(\mathbf{r})$ represents the two-body interaction potential. The dipole motion can be excited by suddenly imposing a finite velocity or displacement to the BEC. In this work we study the same kind of SO-coupling configuration as first realized in Ref. [5], in which $A_x = k_0 \sigma_z$, $A_y = A_z = 0$ and $\Phi = (\delta/2) \sigma_z + (\Omega/2) \sigma_x$. Albeit only one of the three vector-potential components is non-zero, the system still exhibits the non-abelian character because A_x does not commute with the scalar potential Φ . The equation-of-motion for center-of-mass displacement operator $\hat{R}_{\alpha} \equiv (1/N) \sum_{i=1}^N r_{i,\alpha}$ can be derived as

$$\dot{\hat{R}}_{\alpha} = \hat{P}_{\alpha}/m, \quad \ddot{\hat{R}}_{\alpha} = -\omega_{\alpha}^2 \hat{R}_{\alpha} + i[A_{\alpha}, \Phi], \quad \dots, \quad (2)$$

where $\hat{P}_{\alpha} \equiv (1/N) \sum_{i=1}^N (\hat{p}_{i,\alpha} - A_{\alpha})$ is the center-of-mass momentum operator. Along the y or the z direction, because the vector field is zero and $[A_{\alpha}, \Phi] = 0$ ($\alpha = y, z$), the equation-of-motion closes at the second order, and its solution yields a simple solution of harmonic oscillation. While along the x direction, the equation-of-motion cannot close at any finite order because of $[A_x, \Phi] \neq 0$. In fact, it becomes more and more complicated as the order increases. Therefore, *the non-abelian nature of the gauge field gives rise to the prediction that dipole oscillation of a SO-coupled BEC is no longer harmonic.*

Another consideration is about the Galilean invariance. Consider a BEC moving with velocity \vec{v} . In the co-moving frame, the Hamiltonian acquires a term $-\sum_{i=1}^N \vec{v} \vec{p}_i$. Without gauge field, such a term can be gauged away by a gauge transformation $\psi \rightarrow \exp(i \sum_i m v_{\alpha} r_{i,\alpha}) \psi$, and the Hamiltonian is invariant up to a constant of classical energy. With gauge field, the Hamiltonian after gauge transformation becomes

$$\hat{H} = \sum_{i=1}^N \sum_{\alpha=x,y,z} \left(\frac{1}{2m} (\hat{p}_{\alpha,i} - A_{\alpha})^2 - m v_{\alpha} A_{\alpha} + \Phi + \frac{1}{2} m \omega_{\alpha}^2 r_{\alpha,i}^2 + \frac{m v_{\alpha}^2}{2} \right) + \sum_{i<j} U(\mathbf{r}_i - \mathbf{r}_j). \quad (3)$$

For our gauge field configuration, it means that the Hamiltonians in the co-moving frame and in the stationary frame differ by a velocity-dependent Zeeman term $-m v_x k_0 \sigma_z$. Thus, an equilibrium stationary spin configuration cannot remain equilibrium once the condensate

moves. As a result, the polarization $\mathcal{M} = (n_{\uparrow} - n_{\downarrow})/(n_{\uparrow} + n_{\downarrow})$ will oscillate during the dipole oscillation. Hence, *the absence of the Galilean invariance yields the prediction that dipole oscillation will induce magnetization oscillation.*

Our following experiment verifies the above two predictions, and further produces new features that request further theoretical understanding. The experimental layout is sketched in Fig. 1(a). A ^{87}Rb BEC of about 2.5×10^5 atoms is produced in the crossed optical dipole trap, which has a wavelength of 1070 nm and a beam waist of $80\mu\text{m}$. The trap frequency is $\{45,45,55\}$ Hz in the x , y , and z axis, respectively. A bias magnetic field \mathbf{B}_{bias} along the z axis generates the Zeeman splitting. The BEC is illuminated by a pair of linear and circular polarized Raman lasers with beam waist of $240\mu\text{m}$ in the x - y plane and with relative angle $\theta = 105^\circ$. The wavelength of the Raman lasers is chosen as $\lambda = 803.3\text{nm}$, which significantly far off resonance to the ^{87}Rb D_1 or D_2 lines and thus suppresses spontaneous emission. The Raman lasers couple the three internal states of the $F = 1$ manifold via two-photon process, as shown in Fig. 1(b). The single-particle Hamiltonian along the x direction reads ($\hbar = 1$)

$$\hat{H}_0 = \begin{pmatrix} \frac{1}{2m}(k_x + k_r)^2 - \frac{\delta}{2} & \frac{\Omega}{2} & 0 \\ \frac{\Omega}{2} & \frac{1}{2m}(k_x - k_r)^2 + \frac{\delta}{2} & \frac{\Omega}{2} \\ 0 & \frac{\Omega}{2} & \frac{1}{2m}(k_x - 3k_r)^2 + \frac{3\delta}{2} + \epsilon \end{pmatrix} \quad (4)$$

where k_x is the quasi-momentum, Ω is the strength of Raman coupling, δ is the two-photon Raman detuning and ϵ is the quadratic Zeeman shift. Hereby, $k_r = (2\pi/\lambda) \sin(\theta/2)$ is the recoil momentum along the x direction, and $E_r = k_r^2/(2m) = 2\pi \times 2.21\text{kHz}$ ($\hbar = 1$) is the recoil energy; they will be used as the natural units. Digitalization of Eq. (4) yields three different eigenstates for each k_x , in which the spin and the momentum of an atom are locked. In experiment, the BEC is initially prepared at $|F = 1, m_F = -1\rangle$. The Raman lasers are then adiabatically switched on, and the BEC stays at the lowest energy eigenstate. We shall focus on the SO coupling between states $|m_F = -1\rangle$ and $|0\rangle$, which are defined as the spin states $|\uparrow\rangle$ and $|\downarrow\rangle$, respectively. For this purpose, we set the quadratic Zeeman shift as $\epsilon = 3.37E_r$ by applying $\mathbf{B}_{\text{bias}} = 7.2$ Gauss, making the coupling between $|0\rangle$ and $|+1\rangle$ significantly far off resonance. Hence, the physics is qualitatively the same as in a spin-1/2 system. However, for quantitative calculation we should always use the 3×3 Hamiltonian in Eq. (4). By tuning Ω and δ , one can experimentally control the single-particle spectrum. For small coupling Ω and detuning δ , the energy dispersion $\mathcal{E}(k_x)$ has two local minima; while for large Ω or large δ , $\mathcal{E}(k_x)$ has only one minimum. We display in Fig. 1(c) the

phase boundary between the double- and the single-minimum region. In this work, we shall systematically investigate the dipole oscillation by tuning Ω , δ , along paths P_1 , P_2 , and P_3 in Fig. 1(c), of which the single-particle dispersion curves are shown in the insets.

The time sequence for the experiment is shown in Fig. 1(d). After the BEC is prepared in the trap ($t = 0$), the Raman coupling is adiabatically ramped up from zero to Ω in a time period t_1 from 70 to 100 ms, and at the same time the bias magnetic field is gradually switched on, which adiabatically changes the Raman detuning from an initial value $\delta_i > 20E_r$ to an intermediate value δ_m between δ_i and the final value δ_f . At time t_1 , the Raman detuning δ is suddenly switched from δ_m to δ_f , effectively giving the BEC a pulsed momentum. Further, by varying the intermediate two-photon detuning δ_m , one can also excite the dipole oscillation with different oscillation amplitudes. The BEC then starts to oscillate in the trap and is held for a hold time $t_h = t_2 - t_1$. At time t_2 , both the Raman lasers and the optical dipole trap are quickly switched off within $1 \mu\text{s}$. With the Stern-Gerlach technique, a time-of-flight (TOF) image is taken after 24 ms of free expansion, from which the information of spin and momentum is read out. For comparison, an independent experiment without SO coupling is carried out. The Raman lasers are not turned off in the comparison experiment because their presence changes the frequency of the dipole trap. Instead, one sets a sufficiently large detuning $\delta > 20E_r$ to effectively suppress the SO coupling. The time sequence for controlling the Raman lasers and the dipole trap is the same as in the experiment with SO coupling. The difference lies at the control sequence for the bias magnetic field, shown as the red line in Fig. 1(d). The bias field \mathbf{B}_{bias} is first set at $\delta = \delta_f$ at $t = 0$, and at time t_2 is suddenly switched to be far off resonance.

Figure 2 displays the typical oscillations observed in the experiment. We find that, except in the regime marked by yellow in Fig. 1(c), these motions are well described by a single-frequency periodic oscillation. For oscillations along the x direction, clearly the presence of the non-abelian gauge field changes the oscillation frequency. Figure 3(a) shows how the frequency depends on the Raman coupling strength Ω for small and large oscillation amplitude along path P_1 ($\delta = 1E_r$). As the Raman coupling Ω becomes stronger, the derivation from trap frequency becomes larger. Moreover, the oscillation frequency also depends on the oscillation amplitude, as shown in Fig. 3(b) with $\Omega = 4.8E_r$ and $\delta = 1E_r$. These two features clearly demonstrate that the dipole oscillation along the x direction is no longer harmonic. In contrast, for the oscillation along the z direction where there is no

vector potential, the frequency is still the trap frequency and is independent of oscillation amplitude, as shown in the inset of Fig. 3(a).

The magnetization oscillation is also observed clearly in the TOF images with the Stern-Gerlach technique, as shown in Fig. 4(a). We display the oscillation of the quasi-momentum k_x and the polarization \mathcal{M} in Fig. 4(b) and (c), respectively, from which we can see that the frequency of magnetization oscillation is exactly the same as that of the center-of-mass oscillation. To understand their relation better, we take the assumption that the BEC always stays at the lowest eigenstate branch during the entire oscillation, and the spin configuration can adiabatically follow the center-of-mass motion. Thus, for each given time t_h , the quasi-momentum k_x can be read out from the TOF image as in Fig. 4(b), and then the spin wave function $(\cos \theta \sin \varphi, \sin \theta \sin \varphi, \cos \varphi)$ can be calculated by diagonalizing Hamiltonian (4), where both θ and φ are functions of k_x due to the spin-momentum locking. Then one can calculate the polarization as $\mathcal{M} = \cos^2 \theta - \sin^2 \theta$. As shown in Fig. 4(c) the calculated \mathcal{M} value agrees well with \mathcal{M} directly measured from the experiment. This excellent agreement proves that our assumption is a correct physical picture.

Based on this picture we develop a quantitative description of the dipole oscillation with SO coupling using a variational wave-function approach (See Supplementary for details). At the $F = 1$ state, the interaction of ^{87}Rb atoms is nearly $SU(2)$ invariant, and depends on the total density only. The spin-dependent interaction energy is about 0.46% of the total interaction energy [18]. Thus, although the spin configuration is time-dependent, the total interaction energy is nearly a constant. Therefore, in the experiment the dipole oscillation will not excite the surface modes or the breathing modes. This can be shown explicitly with the variational wave-function description. Further, one can show that in the limit of small oscillation amplitude, the oscillation frequency can be calculated by the effective mass approximation. The effective mass is given by $1/m^* = \partial^2 \mathcal{E}(k_x) / \partial k_x^2 |_{k_x=k_0}$, where k_0 is the location of the minimum of $\mathcal{E}(k_x)$, and then $T_x = (2\pi/\omega_x) \sqrt{m^*/m}$. In Fig. 3(b) we show that the effective-mass approximation fits perfectly with the experimental data for small oscillation amplitude. However, for large oscillation amplitude, we need to go beyond this approximation and solve the coupled equation (see Supplementary for details)

$$\dot{p}_x = -\omega_x^2 \xi_x, \quad \dot{\xi}_x = \partial \mathcal{E}(p_x) / \partial p_x, \quad (5)$$

where p_x and ξ_x denote the momentum and position of the center-of-mass, respectively. The

solution of Eq. (5) yields the amplitude dependence of the oscillation frequency, which is compared with experiment in Fig. 3(b).

Measurements have also been performed along paths P_2 and P_3 in Fig. 1(c). The measured oscillation periods are shown in Fig. 5(a) and (b) for P_2 and P_3 , respectively, where the solid lines are the theoretical results by solving Eq. (5). Figure 5(a) suggests that along path P_2 with fixed $\Omega = 3.3E_r$, the agreement with theory becomes worse when δ is close to zero, where two local energy minima in the single-particle spectrum gradually become degenerate. Along path P_3 with fixed $\delta = 0$, we find if the Raman coupling is either large ($\Omega \gtrsim 4E_r$) or small ($\Omega \lesssim 2E_r$), the dipole oscillation is a single-frequency periodic oscillation, and the agreement with theory is very good, as shown in Fig. 5(b). However, as shown in the inset of Fig. 5(b), for an intermediate range of Ω , where the single-particle spectrum gradually changes from a double- to a single-minimum structure, the dipole oscillation becomes quite messy, and cannot be described by a single-frequency oscillation. Thus, we do not have data points in Fig. 5(b) for this regime. These two measurements show that the dipole oscillation is quite complicated in the yellow regime of Fig. 1(c) and the simple variational wave-function description fails. In this regime, the single-particle spectrum has two nearly degenerate minima and the energy barrier between them is comparable to the trap frequency. Hence, macroscopic quantum tunneling occurs between the two minima during the dipole oscillation, which gives rise to more intriguing quantum dynamics.

The interplay between the dipole oscillation and the macroscopic quantum tunneling is a novel feature of this system. Coherent tunneling of superfluid or superconductor between two local minima yields the famous Josephson effect [19]. Several experiments have been carried out to study the Josephson effect of a BEC in a real-space double-well potential [20]. In the SO coupled BEC, the double-well potential is in quasi-momentum space. In this case, the harmonic trapping potential plays an analogous role as the kinetic energy in the real-space double-well potential. As a consequence, the dipole oscillation will cause tunneling between two local minima in the quasi-momentum space when the barrier height is comparable to the trap frequency. For instance, in Fig. 5(c) we plot the atom density distribution in quasi-momentum space $n(k_x)$ as a function of time t_h for $\Omega = 3.5E_r$ and $\delta = 0$. In this case, tunneling between two different quasi-momentum state with nearly the same group velocity (but located in the left and the right well, respectively) are clearly observed twice around 40 ms and 60 ms, and the tunneling points are marked by black triangles in the plot. As time

evolves, the wave packet becomes more and more diffused in the quasi-momentum space. Theoretically, we perform a numerical simulation of the Gross-Pitaevskii equation, and the results are shown in Fig. 5(d). They fairly agree.

In summary, we have experimentally demonstrated that even the simplest dipole oscillation reveals a number of unconventional features in the dynamics of the SO coupled BEC. In the presence of the SO coupling, the dipole mode becomes unharmonic, namely, the frequency deviates from the trap frequency and depends on the oscillation amplitude, revealing the non-abelian nature of the gauge potential. A magnetization oscillation is induced by the dipole motion due to the absence of the Galilean invariance. In the double-minimum region with low barrier, coherent tunneling in the quasi-momentum space occurs during the dipole oscillation. In future, we plan to utilize the dynamics probes to reveal more physics in this system. For instance, in the stripe superfluid phase [5, 9, 10], the stripe order comes from the superposition of condensate wave function with different quasi-momentums, and the dynamics of the relative phase in the superposition plays an important role in the low-energy physics of stripe superfluid. It will be very interesting to study the dynamic properties of the stripe superfluid, including the coupling between different modes and its topological defects. Such a study would greatly enrich our understanding of this novel superfluidity.

HZ would like to thank Sandro Stringari and Lev Pitaevskii for invaluable discussions on collective modes and Josephson effect. This work has been supported by the NNSF of China, the CAS, the National Fundamental Research Program (under Grant No. 2011CB921300, No. 2011CB921500) and NSERC.

-
- [1] D. C. Tsui, H. L. Stormer, and A. C. Gossard, Two-dimensional magnetotransport in the extreme quantum limit. *Phys. Rev. Lett.* **48**, 1559 (1982).
 - [2] For a review, see M. Z. Hasan, C. L. Kane, Topological insulators. *Rev. Mod. Phys.* **82**, 3045 (2010); X.-L. Qi and S.-C. Zhang, Topological Insulators and Superconductors, *Rev. Mod. Phys.* **93**, 1057 (2011).
 - [3] Y.-J. Lin *et al.*, Bose-Einstein condensate in a uniform light-induced vector potential. *Phys. Rev. Lett.* **102**, 130401 (2009); YY.-J. Lin, R. L. Compton, K. Jiménez-García, J. V. Porto, and I. B. Spielman, Synthetic magnetic fields for untracold neutral atoms. *Nature* **462**, 628

- (2009).
- [4] Y-J. Lin *et al.*, A synthetic electric force acting on neutral atoms. *Nature Physics* **7**, 531 (2011).
 - [5] Y-J. Lin, K. Jiménez-García, I. B. Spielman, Spin-orbit-coupled Bose-Einstein condensates. *Nature* **471**, 83 (2011).
 - [6] R. A. Williams *et al.*, Synthetic partial waves in ultracold atomic collisions. *Science* (2011) [DOI: 10.1126/science.1212652].
 - [7] M. Aidelsburger *et al.*, Experimental realization of strong effective magnetic fields in an optical lattice. *Phys. Rev. Lett.* **107**, 255301 (2011).
 - [8] Z.-K. Fu *et al.*, Bose-Einstein Condensate in a light-induced vector potential using the 1064 nm optical dipole trap lasers. *Phys. Rev. A* **84**, 043609 (2011).
 - [9] C. Wang, C. Gao, C. M. Jian, and H. Zhai, Spin-orbit coupled spinor Bose-Einstein condensates. *Phys. Rev. Lett.* **105**, 160403 (2010).
 - [10] T. L. Ho, and S. Zhang, Bose-Einstein condensates with spin-orbit interaction. *Phys. Rev. Lett.* **107**, 150403 (2011).
 - [11] For a review, see H. Zhai, Spin-orbit coupled quantum gases. Preprint available at <http://arxiv.org/abs/1110.6798>.
 - [12] M. H. Anderson, J. R. Ensher, M. R. Matthews, C. E. Wieman, E. A. Cornell, Observation of Bose-Einstein condensation in a dilute atomic vapor. *Science* **269**, 198 (1995); K. B. Davis *et al.*, Bose-Einstein condensation in a gas of sodium atoms. *Phys. Rev. Lett.* **75**, 3969 (1995).
 - [13] F. Dalfovo, S. Giorgini, M. Guilleumas, L. Pitaevskii, and S. Stringari, Collective and single-particle excitations of a trapped Bose gas. *Phys. Rev. A* **56**, 3840 (1997); R. Onofrio *et al.*, Surface excitations in a Bose-Einstein condensate. *Phys. Rev. Lett.* **84**, 810 (2000).
 - [14] A. Altmeyer *et al.*, Precision measurements of collective oscillations in the BEC-BCS crossover. *Phys. Rev. Lett.* **98**, 040401 (2007).
 - [15] C. D. Fertig *et al.*, Strongly inhibited transport of a degenerate 1D Bose gas in a lattice. *Phys. Rev. Lett.* **94**, 120403 (2005).
 - [16] S. Stringari, Collective excitations of a trapped Bose-Condensed gas. *Phys. Rev. Lett.* **77**, 2360 (1996).
 - [17] W. Kohn, Cyclotron resonance and de Haas-van Alphen oscillations of an interacting electron gas. *Phys. Rev.* **123**, 1242 (1961); F. Dalfovo, S. Giorgini, L. P. Pitaevskii, and S. Stringari, Theory of Bose-Einstein condensation in trapped gases. *Rev. Mod. Phys.* **71**, 463 (1999).

- [18] A. Widera *et al.*, Precision measurement of spin-dependent interaction strengths for spin-1 and spin-2 ^{87}Rb atoms. *N. J. Phys.* **8**, 152 (2006).
- [19] B. D. Josephson, Possible new effects in superconductive tunnelling. *Physics Letters* **1**, 251 (1962).
- [20] M. Albiez *et al.*, Direct observation of tunneling and nonlinear self-trapping in a single bosonic Josephson junction. *Phys. Rev. Lett.* **95**, 010402 (2005); S. Levy, E. Lahoud, I. Shomroni, and J. Steinhauer, The a.c. and d.c. Josephson effects in a Bose-Einstein condensate. *Nature* **449**, 579 (2007); L. J. LeBlanc *et al.*, Dynamics of a tunable superfluid junction. *Phys. Rev. Lett.* **106**, 025302 (2011).

Supplementary

We use a variational wave-function approach [S1] to theoretically study the frequency of the dipole mode. Within the mean-field approximation, the motion of a BEC is described by a Lagrangian [S2, S3]

$$\mathcal{L} = \int \left[\Psi^* \left(i \frac{\partial}{\partial t} - \hat{H}_0 - \frac{1}{2} m \omega_\alpha^2 r_\alpha^2 \right) \Psi - c_0 (\Psi^* \Psi)^2 - c_2 (\Psi^* \vec{S} \Psi)^2 \right] d^3 \mathbf{r}, \quad (6)$$

with \hat{H}_0 the single-particle Hamiltonian and \vec{S} the spin-1 representation of Pauli matrix. Based on the experimental observations, we assume that the BEC stays at the lowest eigenstate branch, and further assume a Gaussian wavepacket for center-of-mass motion

$$\Psi = \prod_{\alpha=x,y,z} \psi(r_\alpha) \begin{pmatrix} \cos \theta(p_x) \sin \varphi(p_x) \\ \sin \theta(p_x) \sin \varphi(p_x) \\ \cos \varphi(p_x) \end{pmatrix}, \quad (7)$$

$$\psi(r_\alpha) = \sqrt{\frac{2}{\pi w_\alpha^2}} \exp \left\{ -\frac{(r_\alpha - \xi_\alpha)^2}{w_\alpha^2} + i p_\alpha (r_\alpha - \xi_\alpha) + i \frac{\beta_\alpha}{2} (r_\alpha - \xi_\alpha)^2 \right\}, \quad (8)$$

where the spin wave function is taken as the lowest eigenstate wave function at quasi-momentum p_x . Parameters p_α and ξ_α are the center-of-mass momentum and position, respectively, which are a pair of conjugate variables. The surface and the breathing modes are described by another pair of conjugate variables, w_α^2 and β_α , respectively. With this

variational wave function, the Lagrangian becomes

$$\mathcal{L} = \sum_{\alpha=x,y,z} \left(p_{\alpha} \dot{\xi}_{\alpha} - \frac{w_{\alpha}^2}{8} \dot{\beta}_{\alpha} - \frac{1}{2w_{\alpha}^2} - \frac{\beta_{\alpha}^2 w_{\alpha}^2}{8} - \frac{1}{2} \omega_{\alpha}^2 \xi_{\alpha}^2 - \frac{1}{8} w_{\alpha}^2 \omega_{\alpha}^2 \right) - \mathcal{E}(p_x) - \frac{\hbar^2(p_y^2 + p_z^2)}{2m} + \frac{c_0 + c_2(1 - f(\theta, \varphi))}{2\sqrt{\pi^3} w_x w_y w_z}, \quad (9)$$

with

$$f(\theta, \varphi) = \sin^4 \theta \sin^4 \varphi + 4 \cos^2 \theta \cos^2 \varphi \sin^2 \varphi - 4 \cos \theta \sin^2 \theta \cos \varphi \sin^3 \varphi.$$

It can be seen that only the c_2 -term couples the dipole oscillation with the surface and breathing modes. However, for ^{87}Rb at the $F = 1$ state, c_2 is only 0.46% of c_0 [18]. Unless the frequencies of different collective modes are accidentally at resonance, it can be shown that the surface and breathing modes induced by the dipole oscillation are too small to be observed in the current experiment, and the feedback effect to the dipole mode frequency is also negligible [S4]. Thus, one can safely ignore the c_2 term. The dipole motions along different directions are decoupled, and further decoupled from other modes. Along the x direction, Eq. (9) yields a coupled equations for p_x and ξ_x , shown as Eq. (5) in the main text. If the oscillation amplitude is small, we can further approximate $\partial \mathcal{E}(p_x) / \partial p_x = (p_x - p_0) / m^*$, where p_0 is the quasi-momentum at the energy minimum. This leads to the effective-mass approximation. Such an approximation fails either for large oscillation amplitude or for large effective mass. In this case, one can obtain the frequency by solving the coupled equations of Eq. (9).

-
- [S1] V. M. Pérez-García, H. Michinel, J. I. Cirac, M. Lewenstein, and P. Zoller, Low energy excitations of a Bose-Einstein condensate: a time-dependent variational analysis. *Phys. Rev. Lett.* **77**, 5320 (1996).
- [S2] T. L. Ho, Spinor Bose Condensates in Optical Traps, *Phys. Rev. Lett.* **81**, 742 (1998).
- [S3] T. Ohmi and K. Machida, Bose-Einstein Condensation with Internal Degrees of Freedom in Alkali Atom Gases, *J. Phys. Soc. Jpn.* **67**, 1822 (1998).
- [S4] Z. Chen and H. Zhai, Collective modes of spin-orbit coupled Bose-Einstein condensate, in preparation.

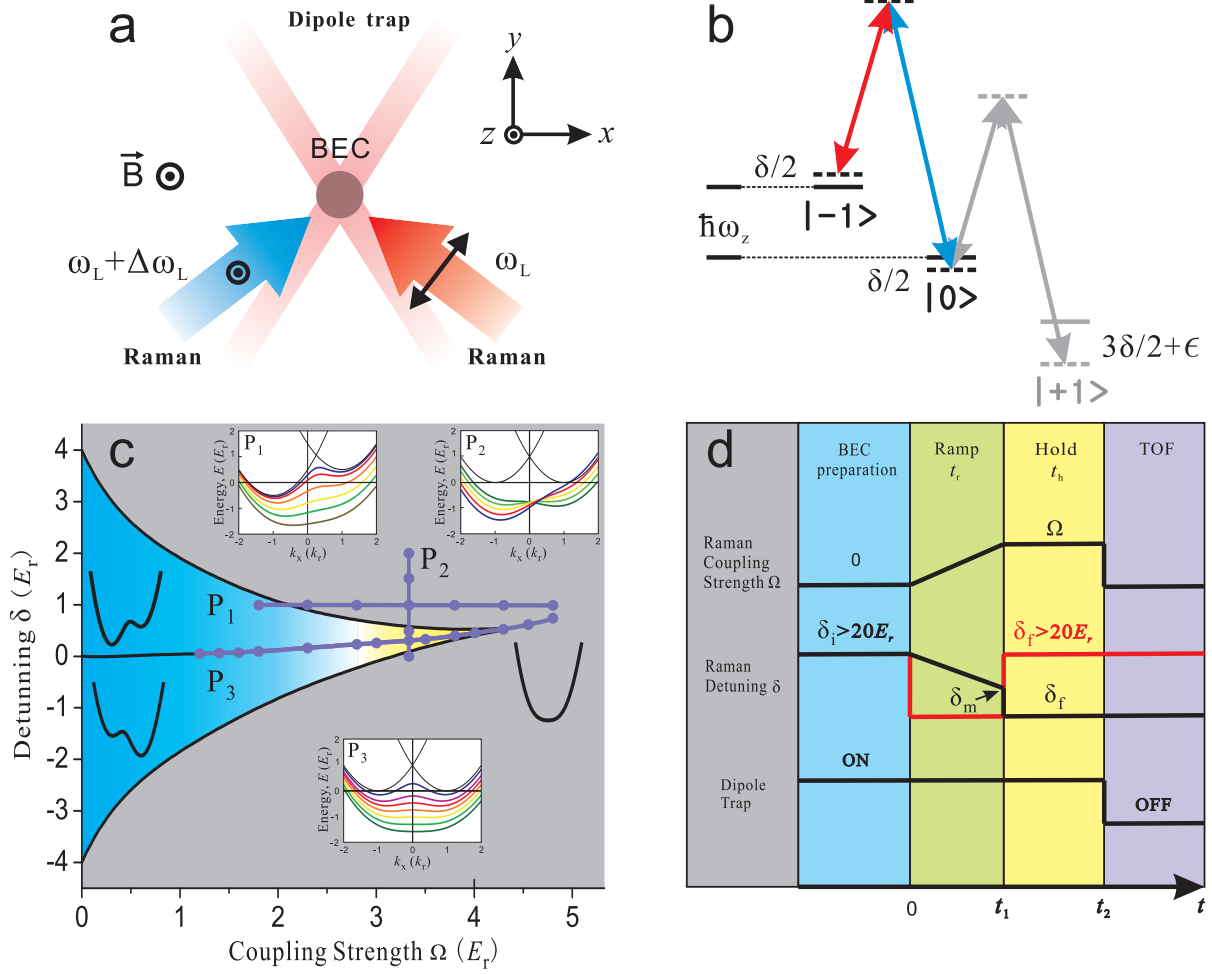


FIG. 1: Experimental summary. (a) Schematic experimental layout. The magnetic field is along the z direction and a pair of counter-propagating Raman lasers are in the x - y plane. (b) Raman coupling scheme within the $F = 1$ manifold. The quadratic Zeeman shift ϵ is set sufficiently large such that state $|+1\rangle$ plays a perturbative role. (c) Single-particle phase diagram in the Ω - δ plane. In the blue regime there are two local minima in the single-particle spectrum, while in the grey regime there is only one minimum. Experiments are carried out along paths P_1 , P_2 , and P_3 , of which the single-particle dispersion curves are shown in the insets. (d) Time sequence for the dipole-oscillation experiment.

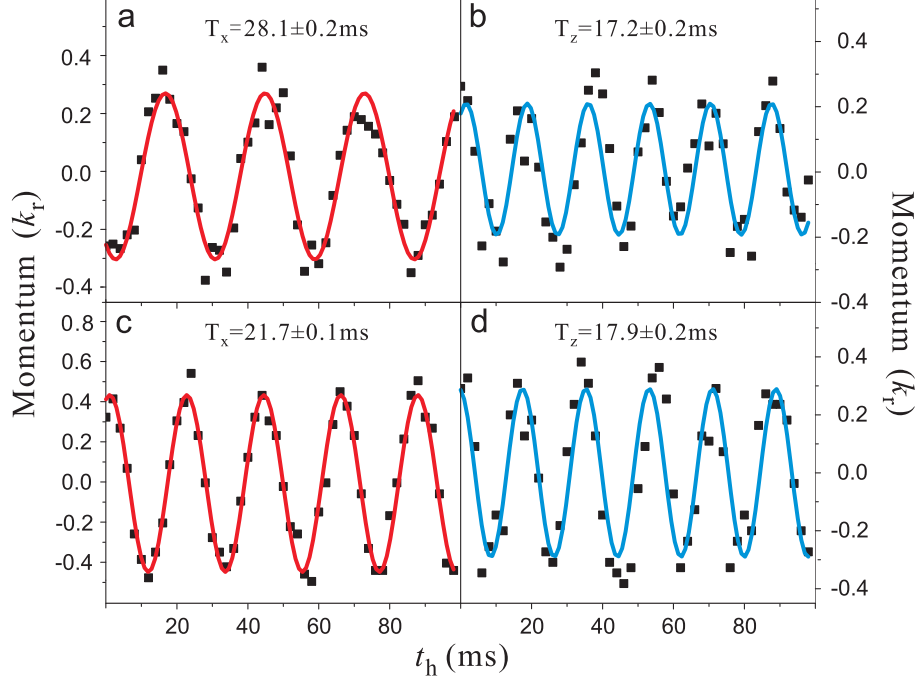


FIG. 2: Momentum as a function of time. (a,b), Oscillation with SO coupling ($\delta = 1E_r$, $\Omega = 3.3E_r$). (c,d), Oscillation without SO coupling ($\delta = 20E_r$, $\Omega = 3.3E_r$). (a,c), Along the the x direction. (b,d), Along the the z direction.

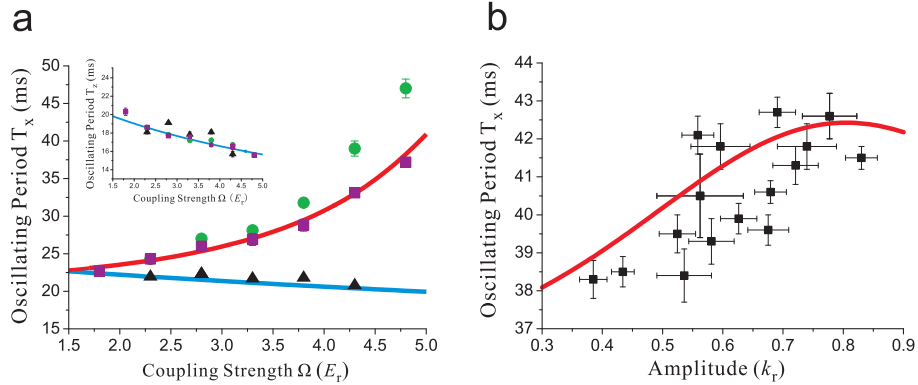


FIG. 3: Dipole oscillation period along path P_1 . (a), T_x versus Ω . The black triangles are for the far-detuned case, and the blue line denotes the estimated trap frequency in presence of Raman lasers. The purple squares (green circles) are for relatively small (large) oscillation amplitude, and the red line is obtained from the effective-mass approximation. The inset is for T_z versus Ω . (b), T_x versus oscillation amplitude with $\Omega = 4.8E_r$. The black squares with error bars are experimental data, and the red line is the theory curve by solving Eq. (5). The two-photon detuning is set at $\delta = 1E_r$ for both (a) and (b).

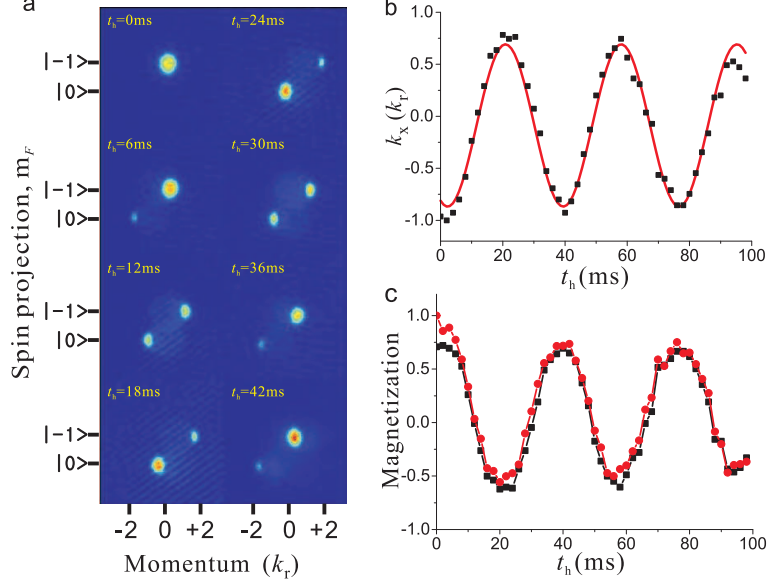


FIG. 4: Magnetization oscillation. (a), Spin-resolved TOF images for different holding times. (b), Quasi-momentum of the center-of-mass motion as a function of holding time t_h . (c), Polarization \mathcal{M} versus t_h . The red circles are from direct measurement, while the black squares are deduced from the measurement of quasi-momentum (see text for detail explanation). Parameters are $\delta = 1E_r$ and $\Omega = 4.8E_r$ for all the plots.

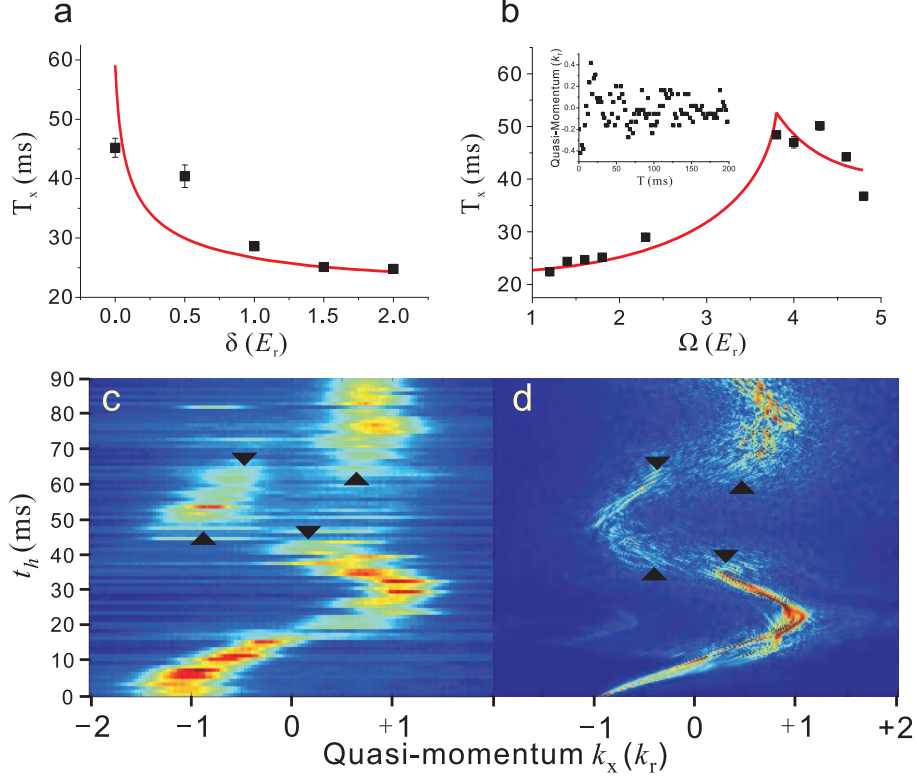


FIG. 5: Quantum tunneling during the dipole oscillation. (a), T_x versus δ along path P_2 , with $\Omega = 3.3E_r$. The black squares are experimental results, and the red line is from the variational wave-function calculation. (b), T_x versus Ω along path P_3 , with $\delta = 0$. The inset displays the dipole motion for $\Omega = 3.3E_r$. (c-d), Monitoring how the condensate wave function in quasi-momentum space evolves as a function of time. (c) is the experimental result and (d) is numerical simulation. The solid black triangles mark the place that quantum tunneling occurs. Parameters are $\Omega = 3.5E_r$ and $\delta = 0$.